Available online at www.sciencedirect.com
ScienceDirect
Solar Energy 84 (2010) 1382–1396
SOLAR ENERGY
www.elsevier.com/locate/solener

Experimental analysis of thermal performance of flat plate and evacuated tube solar collectors in stationary standard and daily conditions

E. Zambolin, D. Del Col *

Dipartimento di Fisica Tecnica, Università degli Studi di Padova, Via Venezia 1, 35131 Padova, Italy

Received 3 June 2009; received in revised form 20 April 2010; accepted 26 April 2010
Available online 11 June 2010

Communicated by: Associate Editor Brian Norton

Abstract

New comparative tests on two different types of solar collectors are presented in this paper. A standard glazed flat plate collector and an evacuated tube collector are installed in parallel and tested at the same working conditions; the evacuated collector is a direct flow through type with external compound parabolic concentrator (CPC) reflectors.

Efficiency in steady-state and quasi-dynamic conditions is measured following the standard EN 12975-2 and it is compared with the input/output curves measured for the whole day.

The first purpose of the present work is the comparison of results in steady-state and quasi-dynamic test methods both for flat plate and evacuated tube collectors. Beside this, the objective is to characterize and to compare the daily energy performance of these two types of collectors. An effective mean for describing and analyzing the daily performance is the so called input/output diagram, in which the collected solar energy is plotted against the daily incident solar radiation. Test runs have been performed in several conditions to reproduce different conventional uses (hot water, space heating, solar cooling).

Results are also presented in terms of daily efficiency versus daily average reduced temperature difference: this allows to represent the comparative characteristics of the two collectors when operating under variable conditions, especially with wide range of incidence angles.

Keywords: Flat plate collector; Evacuated tube collector; Efficiency; Quasi-dynamic method; Daily efficiency

1. Introduction

Mainly two types of liquid solar collectors for domestic heating and hot water production are used presently: flat plate collectors and evacuated tube collectors. They are characterized by different cost and performance, so it is very important to choose the right collector for each application in order to optimize the behaviour of the whole system, the energy savings and the finance payback.

Glazed flat plate collectors usually present a metal absorber in a flat rectangular housing. The glass cover on the upper surface and the insulation on the other side limit the thermal losses. The solar energy absorbed by the plate is transferred to the liquid flowing within the collector tubes. The tubes are in good thermal contact with the absorber surface. Air is present in the space between the plate absorber and the transparent cover. In comparison, evacuated tube collectors allow to reduce the convection and the conduction thermal losses. This collector consists of glass vacuum-sealed tubes; the absorber surface is located into the inner glass tube and it can have several shapes.

* Corresponding author. Tel.: +39 0498276891; fax: +39 0498276896.
E-mail address: davide.delcol@unipd.it (D. Del Col).

0038-092X/$ - see front matter © 2010 Elsevier Ltd. All rights reserved.
doi:10.1016/j.solener.2010.04.020

Nomenclature

A_a	aperture area of collector (m^2)
a	heat loss coefficient for linear regression, Eq. (5) ($W/(m^2\,K)$)
a_1	heat loss coefficient, Eq. (4) ($W/(m^2\,K)$)
a_2	temperature dependence of the heat loss coefficient, Eq. (4) ($W/(m^2\,K^2)$)
b_0	incidence angle modifier coefficient for FPC and for longitudinal projection of angle θ in ETC (–)
b_1, b_2, b_3, b_4	incidence angle modifier coefficients in Eq. (10) (–)
c	heat loss coefficient for daily linear regression, Eq. (11) ($W/(m^2\,K)$)
c_1	heat loss coefficient, Eq. (6) ($W/(m^2\,K)$)
c_2	temperature dependence of the heat loss coefficient, Eq. (6) ($W/(m^2\,K^2)$)
c_3	wind speed dependence of heat loss coefficient, Eq. (6) ($J/(m^3\,K)$)
c_4	long-wave irradiance dependence of the heat loss coefficient, Eq. (6) ($W/(m^2K)$)
c_5	effective thermal capacitance, Eq. (6) ($J/(m^2\,K)$)
c_6	wind speed dependence in the zero loss efficiency, Eq. (6) (s/m)
E_L	long-wave irradiance ($\lambda > 3$ μm) (W/m^2)
ETC	evacuated tube collector
F'	collector efficiency factor (–)
FPC	flat plate collector
G	global solar irradiance (W/m^2)
G_b	direct solar irradiance (W/m^2)
G_d	diffuse solar irradiance (W/m^2)
K_θ	incidence angle modifier for global radiation (–)
$K_{\theta b}$	incidence angle modifier for direct radiation (–)
$K_{\theta d}$	incidence angle modifier for diffuse radiation (–)
$K_{\theta l}$	longitudinal incidence angle modifier (–)
$K_{\theta t}$	transversal incidence angle modifier (–)
$\dot{m}, m$	mass flow rate (kg/s)
n	number of recording time intervals (–)
$\dot{Q}$	useful power extracted from collector (W)
Q_{in}	daily irradiated energy over unitary area (J/m^2) (in the graphs (kWh/m^2))
Q_{out}	daily collected energy over unitary area (J/m^2) (in the graphs (kWh/m^2))
T_a	ambient or surrounding air temperature (K)
t_a	ambient or surrounding air temperature (°C)
t_{in}	inlet temperature to the collector (°C)
T_m	mean liquid temperature (K)
t_m	mean liquid temperature (°C)
T^*_m	reduced temperature difference (m^2 K/W)
T^{*m}_m	daily average reduced temperature difference (m^2 K/W)
t_{out}	outlet temperature from the collector (°C)
U	overall heat loss coefficient ($W/(m^2\,K)$)
u	surrounding air speed (m/s)
$\Delta\tau$	time interval (s)
η	efficiency (–)
η_0	zero loss collector efficiency (η at $T^*_m = 0$) (–)
σ	Stefan–Boltzmann constant ($W/(m^2\,K^4)$)
$(\tau\alpha)$	effective transmittance–absorptance product (–)
$(\tau\alpha)_{en}$	effective transmittance–absorptance product at normal incidence (–)
θ	angle of incidence (°)
θ_t	transversal projection of angle θ (°)
θ_l	longitudinal projection of angle θ (°)

The evacuated tube collectors may be subdivided in two types. In the direct flow through collector the heat transfer liquid is pumped in the tubes. The second type consists of heat pipes inside vacuum sealed glass tubes. A reflector can be present to optimize the absorption of the solar radiation.

The choice of the optimal collector depends on the temperature level required by the specific application and on the climatic conditions of the site of installation. Therefore, in terms of efficiency, each collector displays features which make it most suitable to a certain application.

In conventional uses solar collectors can provide energy for domestic hot water or space heating in combination with low water temperature systems (approximately 35–50 °C), whereas this heat has to be provided above a minimum temperature of 75–80 °C in absorption cooling machines (Schmid et al., 1984). In areas with high sunshine, solar collectors could also be used in cooking process (Hussein et al., 2008) or in still plants (Badran et al., 2005).

The knowledge of the thermal performance of a solar collector is essential to make the right choice. With the publications of the European Standard EN 12975-2 a unique standard exists throughout Europe for solar thermal collector testing. This standard specifies a reproducible procedure and guarantees thus comparable results. It includes two alternative test methods for the thermal performance characterization of solar collectors: steady-state and quasi-dynamic tests.

Some studies on the performance of flat plate collectors following EN 12975 (Kratzenberg et al., 2005; Fisher et al., 2004) and the comparison of uncertainty calculation methods of this performance (Kratzenberg et al., 2006) can be found in the literature. Comparative studies between different normalized test methods for flat plate collectors are also reported in Rojas et al. (2008) and Cucumo et al. (2008). Instead, limited results are available on transient test methods applied to evacuated tube collectors. In (Rönnelid et al., 1997) data from outdoor testing has been used for characterizing the behaviour of a CPC collector with incidence angle; in Perers (1997) the extended MLR procedure is applied to quasi-dynamic method for characterization of evacuated tube collectors

and other collectors with non-linear optical and thermal performance.

Sets of results deriving from the steady-state and quasi-dynamic test methods should be fully comparable between them and allow to draw efficiency curves. However these efficiency curves do not necessarily represent the usual operating conditions and do not describe the global performance of the collector for the entire day.

Long-term performance predictions would allow the comparison between different collectors in several conditions. These predictions are provided by softwares using the parameters obtained from the tests. It is also possible to predict the short-term thermal performance of a solar energy collector under transient operating conditions by means of the overall response function (Prapas et al., 1988), provided that ad hoc measurements are performed.

In this paper the authors present a new set of data collected at Padova, Italy (45°25′N, 11°53′E): both flat plate and evacuated tube collectors are tested simultaneously. For this purpose, steady-state and quasi-dynamic efficiency tests following the standard EN 12975-2 have been performed.

To the best of our knowledge, there is very limited information in the literature regarding the application of the EN 12975 procedure to ETCs. The present paper proposes an example of deriving the incidence angle modifier of ETCs from quasi-dynamic tests.

Extensive data have also been collected in dynamic conditions to evaluate the performance of the collectors in the whole day (daily tests), at various conditions: the experimental results have been reported in the so called input/output diagrams, where the daily useful collected energy is plotted against the daily solar irradiation.

This approach allows a more comprehensive comparison of the effective performance of the two types of solar thermal collectors considered here.

Experimental data taken in the entire day are also used to determine a daily efficiency for both type of collectors. Collector efficiency is a single parameter that combines collector and system characteristics, therefore its values must be carefully handled. The definition of a daily mean efficiency, as compared to steady-state efficiency, allows to enlighten and quantify the advantage or disadvantage of different collectors provided that the test conditions are clearly defined on a bounded test variable space.

2. Experimental apparatus

The experimental apparatus is located on the terrace roof of the Dipartimento di Fisica Tecnica of the University of Padova (Del Col and Padovan, 2007). The apparatus has been set up to allow the measurement of solar collectors efficiency in agreement with the main guidelines of the standard EN 12975-2. Two types of collectors are installed: evacuated tube collector (ETC) and standard glazed flat plate collector (FPC). The FPC system is made of two collectors with connected hydraulic header tubes. The size of the collectors is typical for domestic hot water applications in northern Italy. The collectors are oriented 10° south-west and it is possible to vary the tilt angle.

The flat plate collectors have a copper absorber surface, covered by a selective coating, with 10 parallel cooper tubes, whereas the evacuated tube collector is a direct flow type composed by 21 tubular glasses, with external CPC (compound parabolic concentrator) reflectors.

Fig. 1 shows a picture of the collectors. In Table 1 some characteristics of the collectors installed here are reported (the flat plate collectors area is the total area of the two collectors).

A schematic view of the test loop is reported in Fig. 2. A mixture of water and propylene glycol is used as working fluid to prevent freezing during the winter season. The hydraulic loop is divided in two lines: the first one goes to the flat plate collectors and the second one goes to the evacuated tube collector. Two pumps are used to circulate the liquid. Before entering the collectors, the fluid temperature is controlled in the storage 2, where four electrical heaters are located. Each heater has an electrical power of 5 kW. A control system, connected to a temperature sensor inserted in the storage, acts on these heaters to ensure an accurate control of the liquid temperature at the inlet of the collectors. The liquid temperature at the inlet and at the outlet of the collectors is measured by RTDs (platinum resistance thermometers), both for the flat plate and the evacuated types. The fluid, coming from the collectors, enters the storage 1 and then goes to a plate heat exchanger which works as a heat sink. In the plate heat exchanger the heat flow rate provided by the solar radiation is taken away

Fig. 1. Collectors installed in the test apparatus.

Table 1
Characteristics of the collectors installed in the test rig.

	Plate collectors (m^2)	Evacuated collector (m^2)
Gross area	5.16	3.9
Aperture area	4.76	3.5

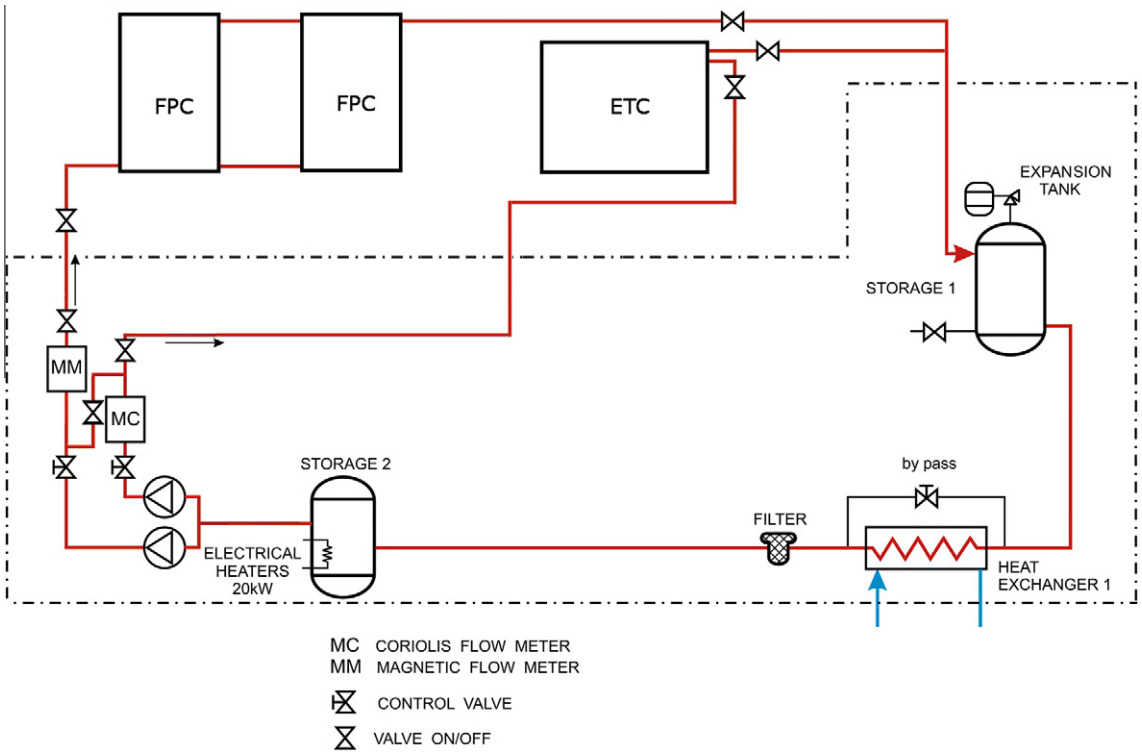

Fig. 2. Schematic view of the experimental test rig.

by a secondary fluid, which is again a mixture of water and propylene glycol. The heat flow rate is wasted in a second plate heat exchanger to the ground water of the building central plant.

Three all black thermopile based pyranometers are used to measure the solar irradiance. A Kipp & Zonen pyranometer, classified as secondary standard by the World Meteorological Organization (WMO), measures the solar irradiance on the plane of the collectors. Other two measurements are taken on the horizontal plane: a first class pyranometer measures the global solar irradiance on the horizontal plane; the third pyranometer (first class classified), shaded against the direct solar radiation, measures only the diffuse component.

A Coriolis effect and a magnetic type flow meters are used to measure the fluid flow rates. The second instrument measures a volumetric flow rate, thus the density of the mixture must be known. For the calibration of the test rig, the two flow meters can be connected in series: this allows checking the measurements obtained by the magnetic flow meter using the more accurate Coriolis effect sensor.

Measurements are possible on both the flat plate and evacuated collectors at the same time. A Copper–constantan thermocouple is used to measure the ambient temperature. Finally an anemometer measures the air speed, being a parameter that influences the heat loss from the collector. In Table 2 the uncertainty of the transducers installed in the test apparatus is reported. The percentages in this table are referred to the measured values.

3. Efficiency in steady-state conditions

During steady-state operating conditions, the useful output power of a solar collector for near normal incidence angle of the solar radiation can be written as reported in Duffie and Beckman (2006):

$$\dot{Q} = F' \cdot A_a \cdot \left[(\tau\alpha)_{en} \cdot G - U \cdot (t_m - t_a)\right] \tag{1}$$

where $\dot{Q}$ is the useful output power transmitted to the liquid, F' the collector efficiency factor, A_a the aperture area of collector, $(\tau\alpha)_{en}$ the effective transmittance–absorptance product at normal incidence, G the global solar irradiance, U the overall heat loss coefficient and $(t_m - t_a)$ the difference between the average fluid temperature in the collector t_m and the ambient air t_a.

The efficiency is equal to:

$$\frac{\dot{Q}}{G \cdot A_a} = F' \cdot \left[(\tau\alpha)_{en} - U \cdot \frac{(t_m - t_a)}{G}\right] \tag{2}$$

and thus:

$$\eta = F' \cdot \left[(\tau\alpha)_{en} - U \cdot T_m^*\right] \tag{3}$$

where T_m^* is the reduced temperature difference.

If the heat loss coefficient is considered as the sum of two terms, a constant factor and a second term dependent on the temperature difference between fluid and ambient air $(t_m - t_a)$, the efficiency equation can be written as:

$$\eta = \eta_0 - a_1 T_m^* - a_2 G (T_m^*)^2 \tag{4}$$

Table 2
Uncertainty of the transducers at typical test conditions.

Fluid temperature	±0.05 K
Ambient air temperature	±0.1 K
Coriolis effect flow meter	±0.1%
Magnetic type flow meter	±0.25%
Solar radiation	Secondary standard sensor (collector plane) First class sensor (diffuse and global on horizontal plane)
Air speed	±(0.1 m/s + 1%)

This form is in agreement with that provided by the standard EN 12975 for steady-state tests.

If the a_2 coefficient is assumed to be without statistical significance, a first order equation is obtained, Eq. (5), which means that the overall heat loss is a linear function of the temperature difference between fluid and ambient air.

$$\eta = \eta_0 - aT_m^* \tag{5}$$

In the case of steady-state tests, only high irradiance levels and thus low diffuse fractions are accepted by the standard. Therefore very stable and sunny weather conditions are needed.

The test runs have been performed in agreement with the guidelines of the standard EN 12975-2, apart from the measurement of the wind speed. The following measurements have been acquired: global irradiance on the collector plane, inlet and outlet fluid temperature in the collectors, surrounding air temperature and fluid flow rate. The surrounding air speed has been measured on the side of the test rig, the values are pretty constant, between 0.7 and 1.3 m/s. In the present data, the effect of the wind speed is reduced as compared to the test requirements given by the EN 12975-2 and therefore the present results are comparable to the condition of negligible surrounding air speed.

The liquid mass flow rate has been set as suggested by the standard; each experimental point is obtained by setting a constant fluid temperature at the inlet of the collectors.

A collector is considered to operate in steady-state conditions if the deviation of the experimental parameters is within the range reported in Table 3. The test period includes a pre-conditioning period of at least 15 min, followed by measurement periods of 10 min.

Table 3
Test conditions and permitted deviations for the steady-state tests according to EN 12975.

Parameter	Value	Deviation from the mean
Global radiation G (W/m^2)	>700	±50
Diffuse fraction G_d/G (%)	<30	
Incidence angle beam irradiance (°)	<20	
Inlet fluid temperature (°C)		±0.1
Surrounding air temperature (°C)		±1.5
Mass flow rate (%)		±1
Surrounding air speed (m/s)	2–4	

This procedure has been repeated varying the inlet fluid temperature and finally the results are reported in diagrams plotting the efficiency against the reduced temperature difference.

The regression curve parameters has been obtained by multiple linear regression (MLR), following the procedure reported in the standard EN 12975-2 and discussed in Kratzenberg et al. (2006), Sabatelli et al. (2002), and Mathioulakis et al. (1999), by developing a process in Matlab environment.

Experimental measurements for steady-state tests for both types of collectors are reported in Fig. 3, where the second order curves obtained with the MLR method are also drawn.

For each point in Fig. 3 the experimental uncertainties of the measured efficiency and the reduced temperature difference (95% confidence interval) are reported, as calculated following the instructions provided in ISO (1995) and described in Kratzenberg et al. (2006) for the measured efficiency.

From the comparison between the curves in Fig. 3, plotted for a global irradiance $G = 1000$ W/m^2, it can be observed that the efficiency of the flat plate collector is higher in the case of low values of reduced temperature difference; the opposite occurs when the reduced temperature is higher than 0.037 (m^2 K)/W. This is an expected result for commercial flat plate and evacuated tube collectors: the efficiency of FPC is higher because of the better value of zero loss efficiency; when increasing the reduced temperature difference, the FPC efficiency is penalised by the higher heat loss coefficient.

Assuming a solar irradiance of 1000 W/m^2 and an ambient air temperature of 20 °C, the cross-over point is obtained at an average liquid temperature $t_m = 57$ °C; if

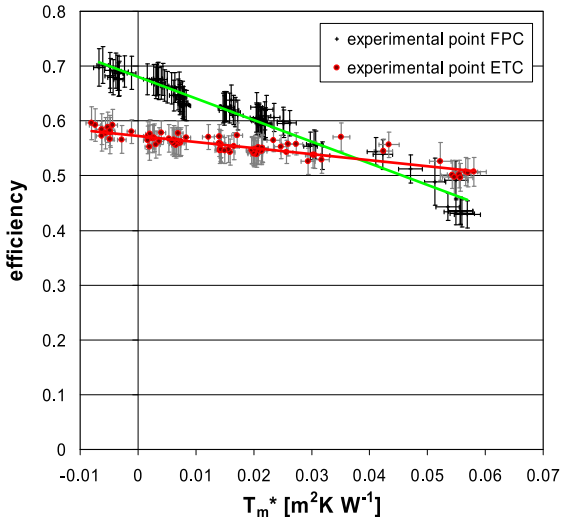

Fig. 3. Efficiency curves at $G = 1000$ W/m^2 and experimental points of evacuated and flat plate collectors obtained in steady-state conditions.

the solar irradiance is 700 W/m^2, the cross-over point increases from 0.037 to 0.038 (m^2 K)/W which means, at the same ambient air temperature, the average liquid temperature decreases to 46.6 °C.

4. Tests in quasi-dynamic conditions

An alternative test method for the thermal performance characterization of solar collectors is the quasi-dynamic method; it allows to achieve comparable results of the steady-state method even at less stable meteorological and operating conditions.

The following is the basic equation for the energy balance of the solar thermal collectors, as reported in the European Standard EN 12975-2:

$$\frac{\dot{Q}}{A_a} = F' \cdot (\tau\alpha)_{en} \cdot K_{\theta b}(\theta) \cdot G_b + F' \cdot (\tau\alpha)_{en} \cdot K_{\theta d} \cdot G_d - c_6 \cdot u \cdot G - c_1 \cdot (t_m - t_a) - c_2 \cdot (t_m - t_a)^2 - c_3 \cdot u \cdot (t_m - t_a) + c_4 \cdot (E_L - \sigma T_a^4) - c_5 \cdot dt_m/d\tau \quad (6)$$

where the coefficients c_i are constant parameters used for the characterization of a solar collector.

In the quasi-dynamic approach the first term of the right-hand side of Eq. (6) is divided into two parts: the zero loss efficiency for beam radiation $F' \cdot (\tau\alpha)_{en} \cdot K_{\theta b}(\theta) \cdot G_b$ and the one for diffuse radiation $F' \cdot (\tau\alpha)_{en} \cdot K_{\theta d} \cdot G_d$.

The wind-dependence is modelled by two correction terms: one term gives the dependence in the zero loss efficiency $c_6 \cdot u \cdot G$, while the term $c_3 \cdot u \cdot (t_m - t_a)$ gives the wind influence of heat losses.

In this model the long-wave "thermal" irradiance dependence of the heat losses is given by $c_4 \cdot (E_L - \sigma T_a^4)$ and the effective thermal collector capacitance term is expressed as $c_5 \cdot dt_m/d\tau$.

The coefficients c_6, c_3 and c_4 can be assumed to be without statistical significance for covered solar collectors (EN 12975-2), where the wind and the long-wave irradiance losses are neglected; thus the c_1 and c_2 terms are equivalent to a_1 and a_2 in Eq. (4). Furthermore, as previously stated, the present data are characterized by negligible surrounding air speed.

4.1. Incidence angle modifiers

For flat plate collectors with flat covers, the angular dependence of the incidence angular modifier is given by:

$$K_{\theta b} = 1 + b_0 \cdot \left(\frac{1}{\cos(\theta)} - 1\right) \quad (7)$$

where b_0 is the incidence angle modifier coefficient (Rönnelid et al., 1997) (negative value). Eq. (7) is used to expand the first term in the collector model expression (Eq. (6)).

For evacuated tube collectors the incidence angle dependence can be much more complicated and $K_{\theta b}$ is not dependent on one single incidence angle θ as in Eq. (7). Instead, the incident beam must be split in two dimensions and the modifier can be described as $K_{\theta b}(\theta_t, \theta_l)$, where θ_t and θ_l are the transverse and longitudinal projection of incidence angle θ, respectively.

For this type of collector it has been suggested (Rönnelid et al., 1997) that the incidence angle modifier can be approximated by the product of two separate incidence angle modifiers:

$$K_{\theta b}(\theta_t, \theta_l) = K_{\theta t}(\theta_t, 0) \cdot K_{\theta l}(0, \theta_l) \quad (8)$$

For the computation of these parameters an ad hoc routine makes it possible to accurately identify non-linear optical performance: in fact the extended MLR method may determine the zero loss efficiency by applying it to small ranges of incidence angle (Perers, 1997). The disadvantage of the extended method is that several regressions must be performed instead of only one. Using the same experimental test data, this may increase the uncertainty of the results due to the lower number of data points in each regression.

In this paper an alternative method is used. The angular dependence of the optical efficiency is assumed to follow a predetermined function. Data points supplied by the manufacturer (Paradigma Energie, Test report of a solar CPC collector) for a similar evacuated tube collector, pertinent to zero loss efficiency, are reported in Fig. 4 as a reference: these data points draw a trend similar to the one reported in Perers (1997), Budihardjo and Morrison (2009). Perers (1997) reports a diagram showing the modifier K_θ versus the incidence angle for a number of different collector designs (including evacuated tube collectors); these results are not obtained with the standard b_0-function, but with the extended MLR. Budihardjo and Morrison (2009) report the transverse incidence angle modifier $K_{\theta t}$ of the water-in-glass evacuated tube collector, which is obtained using experimental measurements and a simulation model.

Here it is assumed that the two modifier parameters can be described as a function of θ_t and θ_l, respectively.

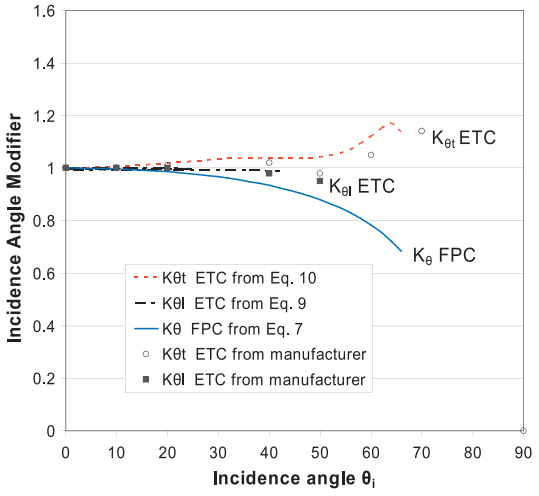

Fig. 4. Incidence angle modifiers obtained from quasi-dynamic tests and values provided by the manufacturer (Paradigma Energie, Test report of a solar CPC collector). $K_{\theta b}$ is the modifier of FPC as defined in Eq. (7) with $\theta_i = \theta$. $K_{\theta l}$ and $K_{\theta t}$ are the modifiers of ETC as defined in Eqs. (9) and (10), with $\theta_i = \theta_l$ and $\theta_i = \theta_t$, respectively.

$$K_{\theta l} = 1 + b_0 \cdot \left(\frac{1}{\cos(\theta_l)} - 1\right) \quad (9)$$

$$K_{\theta t} = 1 + b_1 \cdot \left(\frac{1}{\cos(\theta_t)} - 1\right) + b_2 \cdot \left(\frac{1}{\cos(\theta_t)} - 1\right)^2 + b_3 \cdot \left(\frac{1}{\cos(\theta_t)} - 1\right)^3 + b_4 \cdot \left(\frac{1}{\cos(\theta_t)} - 1\right)^4 \quad (10)$$

where the polynomials are chosen as the minimum order equations able to describe the trend reported in Perers (1997), Budihardjo and Morrison (2009) and the one of the manufacturer's data. The polynomial equation (Eq. (10)) has been selected to keep the same form of Eq. (7) and to provide a curve in agreement with previous studies and manufacturer's data.

A similar procedure is also described in Gaul and Rabl (1980) where the incidence angle modifier is described by a polynomial function of θ.

With regard to the longitudinal incidence angle modifier, $K_{\theta l}$ is a function of $\left(\frac{1}{\cos(\theta_l)} - 1\right)$ with a linear trend like the $K_{\theta b}$ modifier in flat plate geometry and in agreement with Budihardjo and Morrison (2009). Instead, the function of $K_{\theta t}$ is more complex and the 4th order polynomial is necessary to describe its particular trend. This is due to different reflector and envelope losses when varying θ_t, as reported in Kothdiwala et al. (1999).

To accomplish this regression, the polynomial functions of $K_{\theta l}$ and $K_{\theta t}$ expressed as in Eqs. (9) and (10) are implemented in Eq. (6) for the tested evacuated tube collector. It is assumed here that the behaviour of the collector can be described by an M-parameter model, as in Eq. (6), where the unknown terms are the characteristic coefficients of the collector. These parameters have been obtained by multiple linear regression (MLR), following the procedure reported in the standard EN 12975-2 and described in Kratzenberg et al. (2005) and Fisher et al. (2004). A program has been developed in Matlab for the standardized data selection process and the regression step following EN 12975-2.

The quasi-dynamic test method covers a wider range of test conditions as compared to the steady-state test method. In the present selected test data the global solar radiation G ranges between 150 W/m^2 and 1100 W/m^2, the diffuse solar radiation G_d between 33 W/m^2 and 379 W/m^2, the temperature difference $(t_m - t_a)$ between −11 K and 62 K.

As a result, the incidence angle modifiers obtained from the tests are shown in Fig. 4, where $K_{\theta l}$ and $K_{\theta t}$ are reported versus the incidence beam angle along with the values provided by the manufacturer, which are depicted for mere comparison. These curves are reported only in the range covered by the tests, where the modifiers have been experimentally validated. The longitudinal projection of incidence angle in the evacuated collector, θ_l, ranges between 0° and 44° while the transverse projection θ_t goes from 0° to 66° in the tests. It can be seen that $K_{\theta t}$ is higher than one for the whole range of angles in the tests. Comparable trends have been reported in Perers (1997) and Budihardjo and Morrison (2009).

Since the collector tilt and azimuth angle are kept constant during test runs, the longitudinal angle has been varied in a narrow range and therefore the curve of $K_{\theta l}$ reported in Fig. 4 is verified only for incidence angles between 0° and 44°, which corresponds to cos(θ) ranging between 1 and 0.72. The absolute value of b_0 obtained from these tests ($|b_0| = 0.03$) is lower as compared to the usual value reported in the literature, which is about 0.1 (Budihardjo and Morrison, 2009), but this has a minor effect on the efficiency curve due to the limited range of θ_l (at $\theta_l = 44°$ $K_{\theta l} = 0.985$ from the tests, whereas for the same angle $K_{\theta l} = 0.961$ when $|b_0| = 0.1$).

4.2. Efficiency curves

In according to the guidelines of the standard EN 12975-2, the following measurements have been performed during test runs: global irradiance on the collector plane, global and diffuse irradiance on the horizontal plane, inlet and outlet fluid temperature of the collector, surrounding air temperature and fluid flow rates. The incidence angles between direct beam and collector area are calculated for each time step (10 min) for both the FPC and ETC collectors.

The direct and the diffuse radiation on the tilted plane of the collector are calculated from the global radiation measurement on the collector plane and the diffuse radiation measured on the horizontal plane. With regard to the diffuse radiation, the pyranometer is equipped with a shading ring but it is not mounted coplanar with the plane of the collector, as it would be required by EN 12975-2. A correction for the utilization of the shading band is calculated using the Drummond model (Drummond, 1956), to determine the effective diffuse radiation on the horizontal plane, and the Liu–Jordan method (Liu and Jordan, 1963) is then used for calculating the diffuse radiation on the tilted plane of the collector. The direct radiation on the tilted plane is obtained from the difference between global and diffuse radiation on the collector plane.

During each test run the fluid temperature at the inlet of the collectors and the fluid flow rate have been kept constant within about ±1 K and ±1%, respectively. The test

Table 4
Test conditions and permitted deviations for the quasi-dynamic test procedure according to EN 12975.

Parameter	Value	Deviation from the mean
Global radiation G (W/m^2)	>150*	
Inlet fluid temperature (°C)		±1
Outlet–inlet fluid temperature (°C)	>1	
Mass flow rate (%)		±1
Surrounding air speed (m/s)	1–4	

* It is the lower limit in the present tests; EN 12975 does not specify a lower limit for the global radiation.

Table 5
Collector coefficients obtained with quasi-dynamic and steady-state methods for both the collectors.

Parameter	Quasi-dynamic test ETC		Steady-state test ETC		Quasi-dynamic test FPC		Steady-state test FPC	
	Value	Uncertainty	Value	Uncertainty	Value	Uncertainty	Value	Uncertainty
$F'(\tau\alpha)_{en}\ \eta_0$ (sst)	0.5603	±0.0066	0.5718	±0.0044	0.6821	±0.0047	0.6757	±0.0055
b_0	−0.0386	±0.1916			−0.217	±0.022		
$K_{\theta d}$	1.0747	±0.0224			0.9795	±0.0169		
c_1 (W/(m^2 K))	−0.9779	±0.1843	−0.9947	±0.4450	−3.4074	±0.1872	−3.0592	±0.5645
c_2 (W/(m^2 K^2))	−0.0031	±0.0033	−0.002	±0.0093	−0.0143	±0.0036	−0.0228	±0.0116
c_5 (J/(m^2 K))	−24,284	±1027.7			−12,023	±772.8		

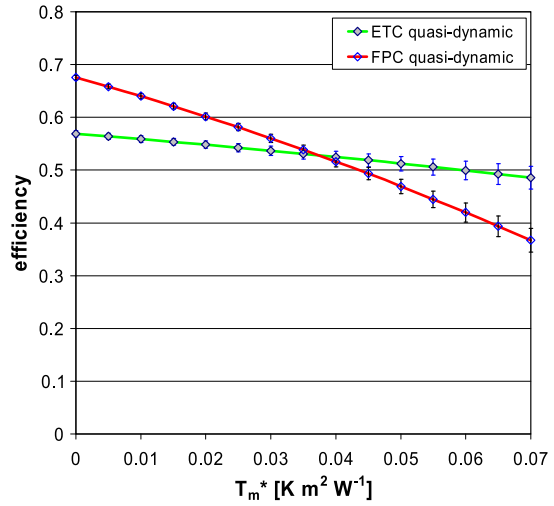

Fig. 5. Efficiency curves of evacuated and flat plate collectors obtained in quasi-dynamic conditions at $G = 1000$ W/m^2.

conditions and the permitted deviation of the measured parameters during quasi-dynamic tests are listed in Table 4.

The test period includes a pre-conditioning period of at least 15 min; instantaneous readings are acquired with a time step of 10 s and are reduced to calculate characteristic mean values for each time interval equal to 10 min.

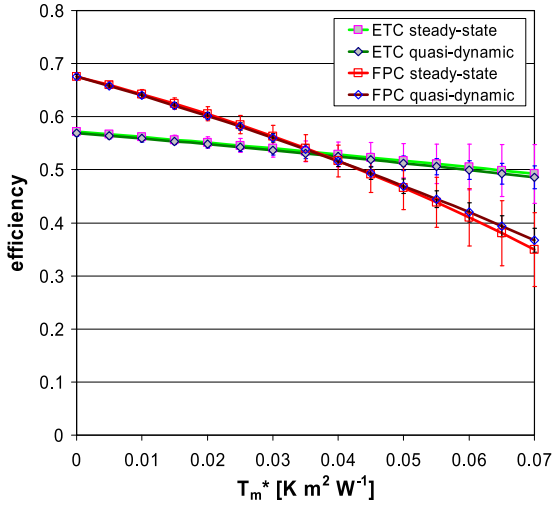

Fig. 6. Compared efficiency curves in steady-state and quasi-dynamic conditions at $G = 1000$ W/m^2.

This procedure has been repeated in different days and for different inlet fluid temperatures; the tests have been performed simultaneously for flat plate and evacuated tube collectors. The parameters of the efficiency curves and their regression uncertainties, determined from the steady-state and quasi-dynamic procedures for both the collector types, are listed in Table 5. In this table the uncertainties of the target parameters are obtained as the square root of the variances, determined as reported in the procedure described in Kratzenberg et al. (2006) in the case of the weighted least square (WLS) method, considering only the variance because all the collector coefficients are uncorrelated.

The efficiency curves, at $G = 1000$ W/m^2 global irradiance, obtained from the present test procedure for both the collector types, are reported in Fig. 5: the uncertainty band (95% confidence interval) is also drawn for some T_m^* values. The uncertainty bands are the expanded uncertainties of the normalized efficiency curves as described in Kratzenberg et al. (2006).

From the comparison between the curves obtained in steady-state and in quasi-dynamic conditions, reported in Fig. 6 for the same irradiance conditions, it can be observed that the results obtained from the two different procedures are fully compatible within their error ranges. Similar agreement between the two collector test procedures is also found in Kratzenberg et al. (2005), Rojas et al. (2008), and Cucumo et al. (2008) and for several flat plate collectors in Fisher et al. (2004).

5. Daily tests

Since optical characteristics and heat losses of these two collectors are very different from each other, the standard stationary efficiency (Section 3) is not sufficient to characterize the distinct behaviour of the collectors. The tests in quasi-dynamic conditions (Section 4) provide a more comprehensive information on the collectors performance. As a further step, daily tests have been performed and analyzed for these two collectors, at the same operating conditions. For the purpose of comparison, the two collectors have worked for the same period of the day, and with the same inlet temperature. This may lead to zero or even negative converted energy for some time: this is accepted here for the purpose of full characterization, although in practical

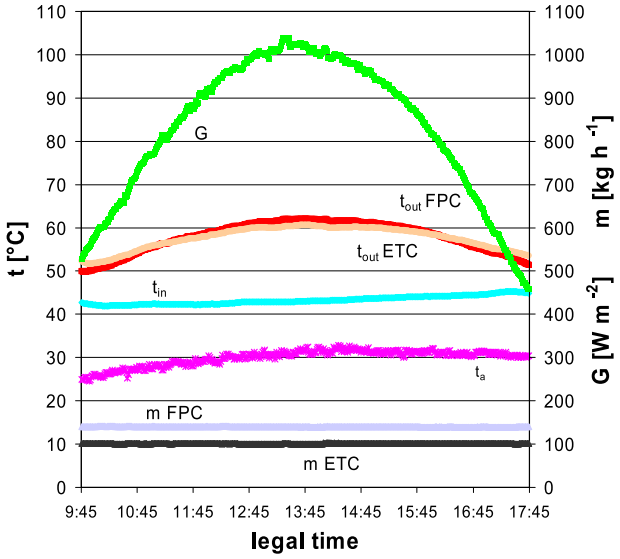

Fig. 7. Measurements during a daily test (July 16, 2008): irradiance, inlet outlet and ambient temperatures, mass flow rate.

applications collectors do not usually work when the heat losses exceed its absorbed solar energy.

For each day the test period ranges between 9:45 a.m. and 5:45 p.m. (legal time). Daily tests have been performed for several environment conditions and different days (sunny, variable, cloudy and rainy conditions): experimental data reported here were measured from July to October 2008 for 30° tilt angle of collectors.

Three different inlet temperatures (about 20, 43 and 73 °C) and fluid flow rates (17, 29 and 50 kg/(m^2 h)) have been investigated.

Characteristic parameters are the incident solar energy on the collector area (input) and the output energy provided by the collectors over 10 min. The entire day is divided in n time intervals of 10 min: the total daily input and output energies are obtained as the sum of the input and the output energy quantities of each time interval. With regard to the output energy, the negative terms are also considered in the sum; this case occurs when the fluid temperature at the outlet of the collector is lower than the inlet temperature, which means that thermal losses are larger than the heat produced by the absorber.

Fig. 7 shows the main parameters recorded during a daily test run for a sunny day (July 16). Flow rate $\dot{m}$ is kept constant for the whole day. The inlet fluid temperature t_{in} of the liquid into the collectors is the same for FPC and ETC. Inlet fluid temperature is roughly constant for the whole day: small variations depend on the ground water used to extract the heat from collectors. Irradiance G and ambient air temperature t_a are also reported.

Outlet temperatures t_{out} vary as dependent on the irradiance conditions. It may be noticed that in the case of the day to which Fig. 7 is referred, the outlet temperature of the flat plate collector overcomes the one of the evacuated tube collector only in the central part of the day.

The collectors' performance for the same day can be seen in Fig. 8, where the measured efficiency during the whole test day is reported for both of the collector types at the same operating conditions (inlet liquid temperature, specific mass flow rate and ambient temperature). In these graphs the reduced temperature is also reported: this parameter has roughly the same value for both collectors.

By knowing the reduced temperature and the efficiency curves of the collectors (Fig. 3) one can calculate the efficiency assuming that the collectors operate constantly at steady-state standard conditions. The calculated values of steady-state efficiency are plotted in Fig. 8a with empty symbols. In the case of ETC, the experimental and calculated efficiencies in Fig. 8a display a similar trend for the

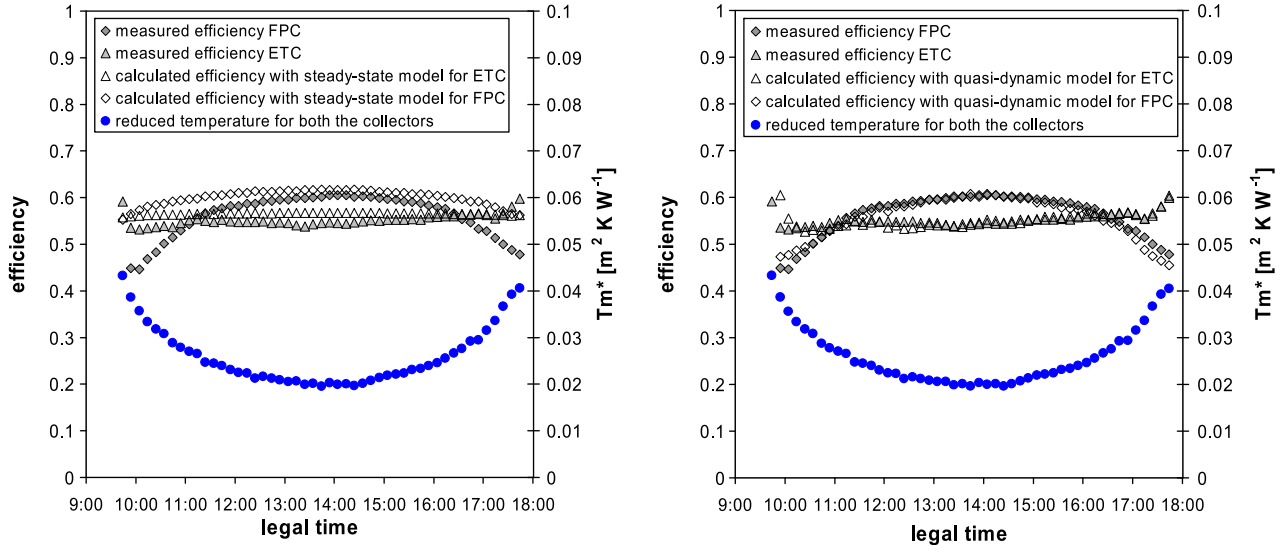

Fig. 8. Comparison between experimental efficiency (solid symbols) and calculated efficiency (empty symbols) during an entire day (July 16, 2008). In Fig. 8a the calculated efficiency is obtained by means of steady-state model, instead in Fig. 8b is obtained by means of quasi-dynamic model.

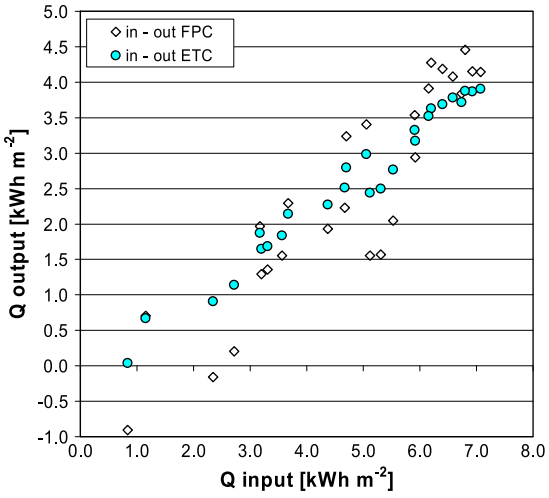

Fig. 9. Experimental points in input–output diagram for both types of collectors.

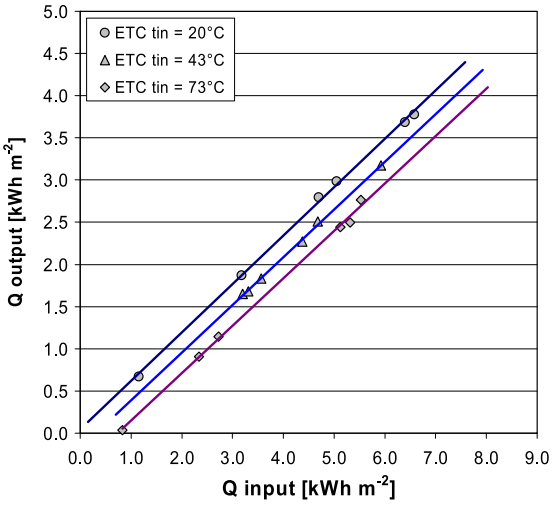

Fig. 10. Input–output diagram of daily energies converted by the evacuated tube collector at three different operating temperatures and constant flow rate (t_{in} is inlet fluid temperature to the collector).

entire day. For FPC, the experimental efficiency is penalized in the morning and evening hours. In fact, in the daily tests, standard conditions requirements (Table 3) are not satisfied. In particular the solar radiation incidence angle varies with time. The effect of incidence angle on the collector performance is usually characterized by means of the parameter K_θ. In Fig. 8a, the difference between measured and estimated efficiency with steady-state model is mainly due to the effect of K_θ in the early and the last hours of the day. In the case of FPC, this parameter (Eq. (7)) is lower than unity if the beam is not perpendicular to the collector plane and therefore the efficiency decreases; on the contrary, for ETC this parameter (Eq. (8)) remains approximately constant along the test period.

In Fig. 8b the same experimental efficiencies are compared to the values computed by means of the quasi-dynamic model. As one would expect, measured and calculated values are in good agreement in this case.

The results obtained in daily tests are plotted in the input/output diagrams (Fig. 9), where the daily incident solar radiation on the collector (x-axis) is related to the daily useful energy (y-axis). An example of a similar procedure is described in Perers et al. (1984).

Fig. 9 illustrates a typical input/output diagram where each energy value is referred to one daily test and to a collector area of 1 m^2. All the experimental points reported in Fig. 9 represent daily collected energies of both collectors and are characterized by different inlet fluid temperature, mass flow rate and environmental conditions. The data scattering is larger for the flat plate collector, as one can see by comparing Figs. 10 and 11, where the data points are reported for the evacuated tube collector and the flat plate collector, respectively, at a constant flow rate of 29 kg/(m^2 h). The test conditions and the main outputs for these daily tests are reported in Table 6.

Experimental points with similar inlet fluid temperatures are grouped together and the regression curves drawn here show a linear trend. The three lines in Figs. 10 and 11 display a medium value of $(\bar{t}_m - \bar{t}_a)$ equal to 0 K, 25 K and 50 K in the case of 20 °C, 43 °C and 73 °C inlet temperature, respectively.

The daily performances of the FPC and the ETC collectors operating in dynamic conditions are compared to each other in Figs. 12–14, at low, medium and high inlet temperature, respectively. It can be seen that these interpolation lines have different slopes for ETC and FPC at the same inlet temperature of the liquid to the collector. This result will be discussed in the following section.

Only at low inlet temperature (Fig. 12), the output energy of the FPC overcomes the one of ETC, because when increasing the fluid-to-ambient temperature difference this leads to larger heat losses and thus larger penalization of the FPC efficiency as compared to the ETC.

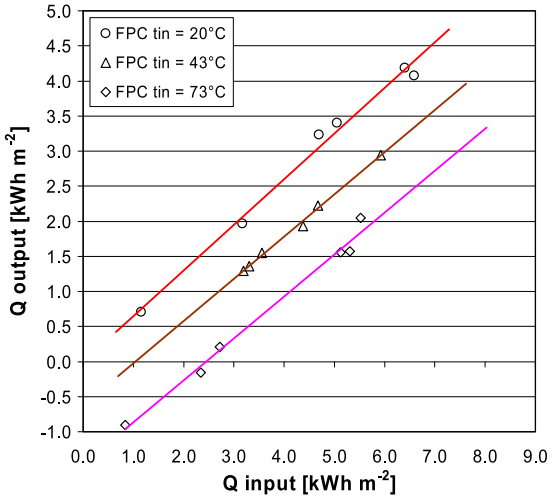

Fig. 11. Input–output diagram of daily energies converted by the flat plate collector at three different operating temperatures and constant flow rate (t_{in} is inlet fluid temperature to the collector).

Table 6
Results obtained for daily tests reported in input/output diagrams.

Data	FPC								ETC								
	Q_{in} (kW h/m^2)	Q_{out} (kW h/m^2)	$\dot{m}/A_a$ (kg/(m^2 h))	$\bar{t}_i$ (°C)	$\bar{t}_m$ (°C)	$\bar{t}_a$ (°C)	$\bar{t}_m - \bar{t}_a$ (K)	$\bar{\eta}$	T^*_m ((m^2 K)/W)	Q_{in} (kW h/m^2)	Q_{out} (kW h/m^2)	$\dot{m}/A_a$ (kg/(m^2 h))	$\bar{t}_i$ (°C)	$\bar{t}_m$ (°C)	$\bar{t}_a$ (°C)	$\bar{t}_m - \bar{t}_a$ (K)	$\bar{\eta}$	T_m*$_m$ ((m^2 K)/W)
10-July	4.70	3.23	29.7	18.9	25.1	30.2	−5.1	0.69	−0.009	4.70	2.80	28.8	18.9	24.4	30.2	−5.8	0.60	−0.010
11-July	6.40	4.19	29.5	27.0	35.0	31.9	3.1	0.65	0.004	6.40	3.68	28.9	27.1	34.2	31.9	2.3	0.58	0.003
11-September	5.05	3.41	29.6	19.7	26.3	31.1	−4.9	0.67	−0.008	5.05	2.98	28.9	19.8	25.6	31.1	−5.5	0.59	−0.009
15-September	3.17	1.97	29.6	19.9	23.7	18.5	5.2	0.62	0.013	3.17	1.87	29.1	20.0	23.7	18.5	5.2	0.59	0.013
16-September	6.58	4.08	29.6	19.9	27.7	21.9	5.8	0.62	0.007	6.58	3.78	29.0	19.9	27.3	21.9	5.4	0.57	0.007
28-October	1.16	0.70	29.5	17.7	19.1	16.4	2.6	0.61	0.018	1.16	0.67	29.2	17.7	19.1	16.4	2.6	0.58	0.018
16-July	6.74	3.84	29.4	43.2	50.5	30.0	20.5	0.57	0.024	6.74	3.72	28.9	43.2	50.4	30.0	20.4	0.55	0.024
17-September	4.68	2.23	29.2	42.6	46.9	20.5	26.4	0.48	0.045	4.68	2.51	29.1	42.6	47.4	20.5	26.9	0.54	0.046
18-September	3.20	1.29	29.2	42.9	45.4	19.0	26.4	0.40	0.066	3.20	1.65	29.0	43.0	46.1	19.0	27.1	0.52	0.068
22-September	5.92	2.94	29.2	43.0	48.7	20.1	28.6	0.50	0.039	5.92	3.17	29.1	43.0	49.1	20.1	29.0	0.54	0.039
09-October	3.56	1.55	29.1	43.8	46.8	21.8	25.0	0.44	0.056	3.56	1.84	29.1	43.7	47.3	21.8	25.5	0.52	0.057
20-October	4.38	1.93	29.1	42.9	46.6	19.0	27.6	0.44	0.050	4.38	2.27	29.1	42.9	47.3	19.0	28.2	0.52	0.052
22-October	3.31	1.36	29.1	42.1	44.7	19.7	25.0	0.41	0.060	3.31	1.68	29.1	42.0	45.3	19.7	25.6	0.51	0.062
10-September	5.52	2.04	29.2	73.9	77.8	30.6	47.2	0.37	0.068	5.52	2.77	28.7	73.7	79.0	30.6	48.4	0.50	0.070
26-September	2.72	0.21	28.9	71.1	71.5	18.6	52.9	0.08	0.156	2.72	1.14	29.1	70.9	73.0	18.6	54.5	0.42	0.160
28-September	5.31	1.57	28.6	72.6	75.6	19.1	56.4	0.30	0.085	5.31	2.50	29.1	72.5	77.3	19.1	58.1	0.47	0.088
30-September	2.34	−0.16	28.6	72.1	71.8	17.7	54.1	−0.07	0.185	2.34	0.91	29.1	71.9	73.7	17.7	56.0	0.39	0.191
10-October	5.12	1.56	28.6	72.1	75.1	22.9	52.2	0.30	0.082	5.12	2.44	29.1	72.0	76.6	23.0	53.6	0.48	0.084
16-October	0.83	−0.91	28.4	71.5	69.7	18.0	51.7	−1.09	0.496	0.83	0.04	28.8	71.3	71.4	18.1	53.3	0.04	0.512

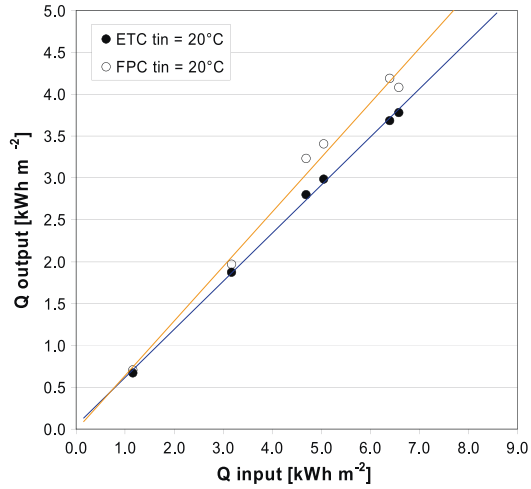

Fig. 12. Comparison of the input–output curves of both collector types at low operating temperatures.

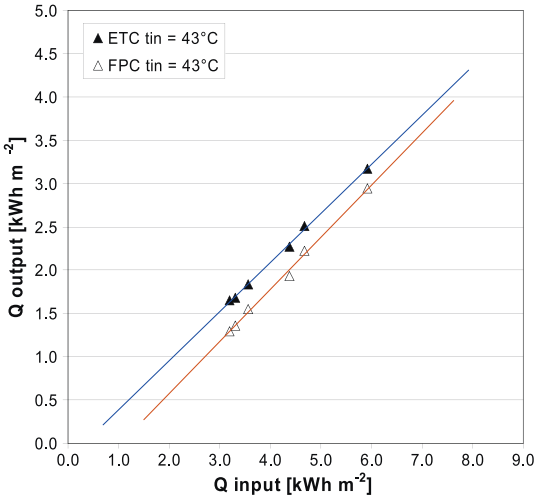

Fig. 13. Comparison of the input–output curves of both collector types at medium operating temperatures.

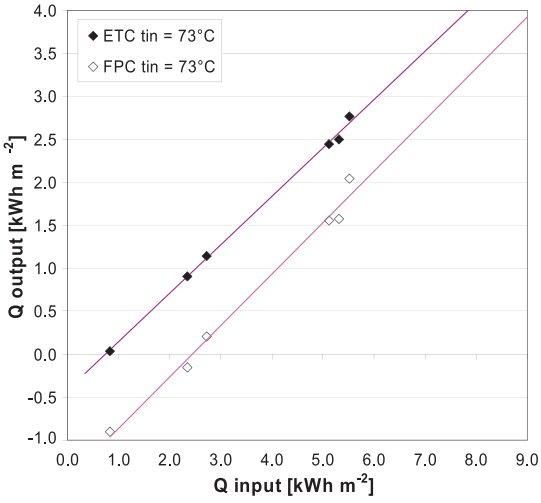

Fig. 14. Comparison of the input–output curves of both collector types at high operating temperatures.

6. Collector model for daily tests

An analytical expression of the daily energy extracted from the collector can be derived from Eq. (6).

The same assumptions described in Section 4 are possible; besides, the radiation term is not splitted into separated sub-models for the direct and diffuse radiation components as it happens in the quasi-dynamic collector model.

As a further simplification, the term $c_2 (t_m - t_a)^2$ is here set equal to zero: in the case of ETCs this assumption is verified because the T-ratio (as defined in EN 12975-2) is lower than 2 (T-ratio = 1.88 in this case) and thus, following the EN 12975-2 criterion, c_2 can be set equal to zero. In the case of FPCs, such a criterion would not allow us to neglect c_2; however $(t_m - t_a)$ is kept within a limited value, around 60 K in the present tests and the product $c_2 (t_m - t_a)^2$ is here neglected as a first approximation. This assumption will be later checked, when plotting the efficiency obtained from daily tests.

Finally, the energy balance in the test period is described by the Eqs. (11) and (12):

$$\int_{n\cdot\Delta\tau} \frac{\dot{Q}}{A_a}\cdot d\tau = \int_{n\cdot\Delta\tau} \left[F'\cdot(\tau\alpha)\cdot G - c\cdot(t_m - t_a) - c_5\cdot\frac{dT_m}{d\tau}\right]\cdot d\tau \tag{11}$$

$$\int_{n\cdot\Delta\tau} \frac{\dot{Q}}{A_a}\cdot d\tau + \int_{n\cdot\Delta\tau} c_5\cdot dT_m = \int_{n\cdot\Delta\tau} F'\cdot(\tau\alpha)\cdot G\cdot d\tau - \int_{n\cdot\Delta\tau} c\cdot(t_m - t_a)\cdot d\tau \tag{12}$$

where the left-hand side is the output energy Q_{out}. This term is calculated by knowing the temperatures trend, the mass flow rate of the collector during the test period and the parameter c_5. The thermal capacitance, reported in Table 7, has been calculated from the quasi-dynamic methods: it does not have an important effect in the present tests, because the inlet temperature is constant during each daily test. For example the thermal capacitance contribution for the FPC in the test day reported in Fig. 7 is lower than 6 W h/m^2 which is only 0.2% of the daily heat production (3836 W h/m^2).

Therefore:

$$Q_{out} = F'\cdot\overline{(\tau\alpha)}\cdot Q_{in} - \int_{n\cdot\Delta\tau} c\cdot(t_m - t_a)\cdot d\tau \tag{13}$$

where:

$$\overline{(\tau\alpha)} = \frac{\int_{n\cdot\Delta\tau}(\tau\alpha)\cdot G\cdot d\tau}{Q_{in}} \tag{14}$$

$\overline{(\tau\alpha)}$ is the average of $(\tau\alpha)$ defined as in Eq. (14) and $n\cdot\Delta\tau$ is the total test period duration.

$$Q_{out} = F'\cdot\overline{(\tau\alpha)}\cdot Q_{in} - c\cdot(\overline{t_m} - \overline{t_a})\cdot n\cdot\Delta\tau \tag{15}$$

$\overline{t}_m$ and $\overline{t}_a$ are the average temperatures over the test period.

Eq. (14) provides an explanation of the experimental trends plotted in Figs. 10–14. In fact, according to the above equation, the output energy is a linear function of the input energy and also depends on the liquid to ambient temperature difference. The slope of the straight lines is due to the parameter $F'\cdot\overline{(\tau\alpha)}$ which is different for the two types of collectors. The flat plate collector displays a higher slope as compared to the evacuated collector, which in turn is due to its higher value of $F'\cdot\overline{(\tau\alpha)}$.

For a given collector, the slope of the input/output energy curves does not vary with the inlet liquid temperature to the collector (see Figs. 10 and 11).

From Eq. (14) it is also possible to obtain an expression of the average collector efficiency during the test period, in agreement with the results obtained by Perers et al. (1984). This equation can be written similarly as in Eq. (5) for steady-state conditions:

$$\frac{Q_{out}}{Q_{in}} = F'\cdot\overline{(\tau\alpha)} - c\cdot\frac{(\overline{t_m} - \overline{t_a})}{\frac{Q_{in}}{n\cdot\Delta\tau}} \tag{16}$$

$$\overline{\eta} = \overline{\eta_0} - c\cdot T_m^{*m} \tag{17}$$

where $\overline{\eta}$ is the average daily efficiency, $\overline{\eta}_0$ is the zero-loss average efficiency and T_m^{*m} is the average reduced temperature, computable by knowing $\overline{t}_m$, $\overline{t}_a$ and Q_{in}.

Therefore, using all the experimental points reported in the input/output diagrams (Fig. 9) the daily efficiency has been calculated. In Fig. 15 the daily efficiency is plotted against the daily average reduced temperature T_m^{*m}; the experimental data and the curves fitting the points are reported.

This data shows a linear trend and this is in agreement with the simplified model presented here; the cross-over point of the regression curves occurs at an average reduced temperature value equal to 0.027 m^2 K/W. Assuming a solar daily irradiated energy of 5.6 kW h/m^2 over 8 h, which means 700 W/m^2 average solar irradiance, and an average ambient air temperature of 20 °C, the cross-over point is obtained for an average fluid temperature $\overline{t}_m$ equal to 39 °C (0.027 m^2 K/W).

Table 7
Efficiency curve parameters.

	Steady-state parameters (second order equation) $\eta = \eta_0 - a_1 T_m^* - a_2 G (T_m^*)^2$			Steady-state parameters (best-fit linear regression) $\eta = \eta_0 - a T_m^*$		Daily parameters (best-fit linear regression) $\overline{\eta} = \overline{\eta}_0 - c\cdot T_m^{*m}$	
	η_0	a_1 (W/(m^2 K))	a_2 (W/(m^2 K^2))	η_0	a (W/(m^2 K))	$\overline{\eta}_0$	c (W/(m^2 K))
FPC	0.676	3.059	0.023	0.680	3.945	0.658	3.950
ETC	0.572	0.995	0.002	0.573	1.111	0.580	1.049

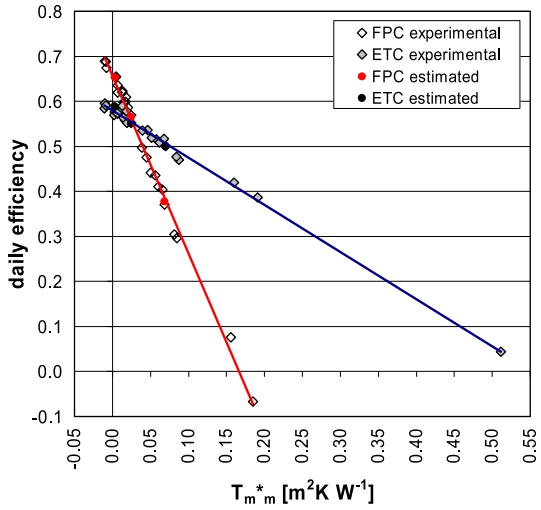

Fig. 15. Daily efficiency curves (best-fit linear regression curves) of the evacuated and flat plate collectors (characteristic parameters defined in Eq. (17); collector constants in Table 7).

Some tests have also been performed at different mass flow rates (low flow and high flow). It is worth mentioning here that when changing the flow rate, the collector efficiency may be different but the experimental points follow the linear trend just found in the daily efficiency diagram. For instance if the mass flow rate decreases, the outlet liquid temperature increases, the mean reduced temperature increases too and the efficiency goes down.

For the sake of comparison, Fig. 15 reports the daily efficiency estimated on three different days from the quasi-dynamic model (Section 4). For each time interval, the efficiency is calculated as in Fig. 8b and the output power is determined as the product $\dot{Q}_{out} = G \cdot A_a \cdot \eta$. By integrating $\dot{Q}_{out}$ over the entire day, one can calculate Q_{out} and the daily efficiency can be reported in Fig. 15. Those estimated values are in agreement with the experimental trends both for FPC and ETC. Therefore, the daily efficiency curve can be well plotted from the parameters determined during tests under quasi-dynamic conditions.

In Table 7 the parameters of the efficiency curves are reported for steady-state (second and first order curves) and daily tests. From the comparison between standard stationary and daily efficiency curves, it can be observed that the zero loss efficiency parameter for evacuated tube collector has the same value for the two data sets. This is due to the K_θ modifier equation: it can be seen in Fig. 4, where the product of $K_{\theta l}$ by $K_{\theta t}$ does not differ much from unity, and in Fig. 8a, where the K_θ trend is described by the difference between the experimental and the calculated efficiency. In the case of the flat plate collector, the zero loss efficiency is lower for the daily tests as compared to the steady-state and quasi-dynamic tests due to the effect of the incidence angle. In the case of the daily curve the incidence angle modifier is lower than unity for most of the time and this explains why the efficiency decreases.

The data points in the daily efficiency curves can be well fitted with a linear function and this verifies the hypothesis to neglect the second order term $c_2 \cdot (t_m - t_a)^2$ in Eq. (5) for average data.

The collector heat loss factor in daily conditions c and in steady-state conditions a, have a similar physical mean. As shown in Fig. 16 and Table 7, for both collectors, roughly the same slope has been found for steady-state and daily tests.

7. Conclusions

Experimental measurements taken on flat plate and evacuated tube collectors are presented here. The efficiency curves have been obtained following the steady-state and the quasi-dynamic methods described by the standard EN 12975-2.

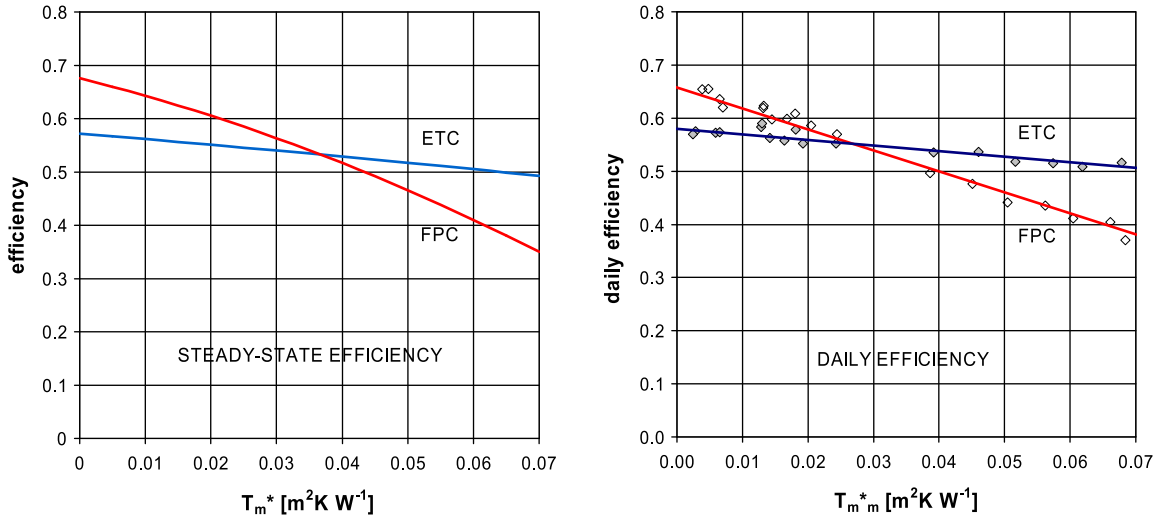

Fig. 16. Efficiency of tested collectors: on the left, efficiency in steady-state conditions as defined in Eq. (4), on the right: daily efficiency as defined in Eq. (17).

The curves obtained with steady-state and quasi-dynamic test methods are in agreement within their uncertainty ranges as shown in Fig. 6: this is true both for FPC and for ETC. For the latter, a particular MLR with predetermined function of $K_{\theta l}$ and $K_{\theta t}$ in the quasi-dynamic method has been used.

Daily test runs are also performed. Input/output diagrams and daily efficiency curves are obtained from these tests. In input/output diagrams, the daily energy collected displays a linear relationship with the daily solar radiation energy, at constant operating temperature difference $(\overline{t}_m - \overline{t}_a)$. As expected, the flat plate collector is more sensitive to this temperature difference than the evacuated tube collector.

A daily efficiency has been defined and plotted versus a daily average reduced temperature for the present test runs. Besides, it was shown that the daily efficiency can be estimated by using the parameters of the quasi-dynamic model.

The daily efficiency can be used to characterize and compare different collectors, once the boundary conditions are declared. For instance, from the comparison between the standard stationary efficiency diagrams and the daily efficiency, two different cross-over points between the evacuated and the flat plate efficiency curves were observed: 0.037 m^2 K/W in standard conditions and 0.027 m^2 K/W in the daily tests (Fig. 16). This difference is essentially due to the variations of $\tau\alpha$ in the daily tests for the evacuated tube and flat plate collectors; in fact the heat loss coefficients (in the first order curve) for both sets of data have roughly the same values.

In the flat plate collector the optical efficiency of the collector in the morning and in the afternoon hours decrease due to more reflection losses. In the vacuum tube collector, these efficiency losses are reduced: because of its geometry the most of the absorber area is exposed to quasi-normal incidence radiation for a longer period of the day. As a result, in the daily tests the evacuated collector displays a higher efficiency for a larger range of operating conditions, as compared to the flat plate collector.

In the present paper the daily efficiency curve is experimentally based and theoretically explained. The collector coefficients obtained from the quasi-dynamic model can be used for the simulation of the yearly energy production in a region with specified climatic characteristics, using for instance Typical Meteorological Year (TMY) (Marion and Urban, 1995), but can also be used to construct a daily efficiency curve which represents an easy-to-use tool for quick evaluation of collectors (without considering the system) in a wide range of operating conditions.

Acknowledgment

The authors would like to acknowledge the financial support of Riello Group through the PhD Grant of Enrico Zambolin.

References

Badran, A.A., Al-Hallaq, A.A., Eyal Salman, I.A., Odat, M.Z., 2005. A solar still augmented with a flat-plate collector. Desalinisation 172, 227–234.

Budihardjo, I., Morrison, G.L., 2009. Performance of water-in-glass evacuated tube solar water heaters. Solar Energy 83, 49–56.

Cucumo, M., Cucumo, S., De Rosa, A., Ferraro, V., Kaliakatsos, D., Marinelli, V., 2008. Comparison between test methods for parameters determination of flat plate solar collectors in transient conditions. In: 63rd ATI Congress (in Italian).

Del Col, D., Padovan, A., 2007. New experimental apparatus for testing the performance of solar collectors. In: 62nd ATI Congress.

Drummond, A.J., 1956. On the measurements of sky radiation. Archiv für Meteorologie Geophysik und Bioklimatologie 7, 413–436.

Duffie, A., Beckman, W.A., 2006. Solar engineering of thermal processes (Chapter 6).

EN 12975-2, 2006. Thermal Solar Systems and Components – Solar Collectors – Part 2: Test Methods.

Fisher, S., Heidemann, W., Muller-Steinhagen, H., Perers, B., Bergquist, P., Hellström, B., 2004. Collector test method under quasi-dynamic conditions according to the European Standard EN 12975-2. Solar Energy 76, 117–123.

Gaul, H., Rabl, A., 1980. Incidence angle modifier and average optical efficiency of parabolic trough collectors. Transactions of ASME, Journal of Solar Energy Engineering 102, 547–551.

Hussein, H.M.S., El-Ghetany, H.H., Nada, S.A., 2008. Experimental investigation of novel indirect solar cooker with indoor PCM thermal storage and cooking unit. Energy Conversion and Management 49, 2237–2246.

ISO, 1995. Guide to the Expression of Uncertainty in Measurement.

Kothdiwala, A.F., Eames, P.C., Norton, B., Zacharopolous, A., 1999. Comparison between inverted absorber asymmetric and symmetric tubular–absorber compound parabolic concentrating solar collectors. Renewable Energy 18, 277–281.

Kratzenberg, M.G., Beyer, H.G., Colle, S., Albertazzi, A., Güths, S., Fernandes, D., Oikawa, P.M.V., Machado, R.H., Petzoldt, D., 2005. Assessment of the Partial Model Stability of the Quasi-Dynamic Collector Test under Outdoor Conditions EN 12975 by the Application of Uncertainty Analysis. In: International Solar Energy Conference, Orlando, USA.

Kratzenberg, M.G., Beyer, H.G., Colle, S., 2006. Uncertainty calculation applied to different regression methods in the quasi-dynamic collector test. Solar Energy 80, 1453–1460.

Liu, B.Y.H., Jordan, R.C., 1963. The long-term average performance of flat-plate solar energy collectors. Solar Energy 7.

Marion, W., Urban, K., 1995. User's Manual TMY2s – Typical Meteorological Year, National Renewable Energy Laboratory, Golden, CO, USA, 1995.

Mathioulakis, E., Voropoulos, K., Belessiotis, V., 1999. Assessment of uncertainty in solar collector modelling and testing. Solar Energy 66, 337–347.

Perers, B., 1997. An improved dynamic solar collector test method for determination of non-linear optical and thermal characteristics with multiple regression. Solar Energy 59, 163–178.

Perers, B., Zinko, H., Holst, P., Eriksson, L., 1984. In: Comparison of the Effective System Performance of Flat Plate and Evacuated Tube Collectors Used for District Heating Purposes in Sweden, vol. 2. Pergamon Press, pp. 1096–1105.

Perers, B., Zinko, H., Holst, P., 1984. Analytical model for the input/output energy relationship. Commission of the European Communities.

Prapas, D.E., Norton, B., Milonidis, E., Probert, S.D., 1988. Response function for solar-energy collectors. Solar Energy 40, 371–383.

Rojas, D., Beermann, J., Klein, S.A., Reindl, D.T., 2008. Thermal performance testing of flat-plate collectors. Solar Energy 82, 746–757.

Rönnelid, M., Perers, B., Karlsson, B., 1997. On the factorisation of incidence angle modifiers for CPC collectors. Solar Energy 59, 281–286.

Sabatelli, V., Marano, D., Braccio, G., Sharma, V.K., 2002. Efficiency test of solar collectors: uncertainty in the estimation of regression parameters and sensitivity analysis. Energy Conversion and Management 43, 2287–2295.

Schmid, R., Collins, R.E., Mannik, E., 1984. Performance comparison of flat plate and evacuated tubular collectors used in the Sydney University solar cooling and heating project. In: Biennial Congress of Int. Solar Energy Society Perth, vol. 2, pp. 1056–1060.